ASME Journal of Dynamic Systems, Measurement, and Control
Online journal at:
https://asmedigitalcollection.asme.org/dynamicsystems

In-Situ Calibration of Six-Axis Force/Torque Transducers on a Six-Legged Robot

Ziyou Wu[1]
Robotics Department,
University of Michigan,
Ann Arbor, MI 48105
e-mail: wuziyou@umich.edu

Shai Revzen
Associate Professor
Electrical and Computer Engineering,
Ecology and Evolutionary Biology,
Applied Physics,
Robotics Department,
University of Michigan,
Ann Arbor, MI 48105
e-mail: shrevzen@umich.edu

Ground contact modeling for multilegged locomotion is challenging due to the possibility of multiple slipping legs. To understand the interplay of contact forces among multiple legs, we integrated a robot with six high-precision 6 degree-of-freedom (DoF) force-torque sensors, and measured the wrenches (forces and torques) produced in practice. Here, we present an in situ calibration procedure for simultaneously measuring all foot contact wrenches of a hexapod using 6-DoF load cells installed at the hips. We characterized transducer offset, leg gravity offset, and the wrench transformation error in our calibration model. Our calibration reduced the root-mean-square-error (RSME) by 63% for forces and 90% for torques in the residuals of the robot standing in different poses, compared with naive constant offset removal. [DOI: 10.1115/1.4066455]

1 Introduction

Force/torque (F/T) transducers are commonly used in robotics applications to sense the interaction between robots and their environment [1]. The simultaneous and accurate measurement of multiple concurrent contact forces through, e.g., a robot's legs, has proven to be a challenging calibration problem, for which we present one solution here. This solution proved effective for performing ground contact measurement on our 8.18 kg, 73 cm long hexapedal robot BigANT.

Force/torque transducers are used in robotic surgery [2], manipulation [3,4], robot locomotion [5–7], etc. Knowing contact forces can allow a robot to sense its surroundings more fully, with ensuing benefits to both planning and control. For legged robots that move by making and breaking contacts with the ground to produce propulsion and load bearing, F/T transducers can measure how the load is distributed among legs. The measurements can reveal how much propulsion each leg produces, and what slipping might occur, and thereby inform modeling and control. Such F/T measurements have been used in contact detection [5], gait modeling [6], state estimation [8], terrain classification [7], maintaining stability [9], and other applications in legged robotics.

Our work was motivated by the goal of understanding the interplay of contact forces while a multilegged robot moves with its feet slipping on the ground. We are particularly interested in multilegged robots with low degree-of-freedom legs [10,11]. The mass of such robots is typically concentrated in the body, allowing fast swinging legs, lower leg collision forces, and smaller energy costs for leg impacts. Our previous work showed that slipping was an essential part of expressing the high maneuverability of these robots [12], but due to a lack of precise contact force measurements, our mechanistic understanding of these complex slipping motions was incomplete. We did manage to reliably model the body velocity resulting from a multilegged slipping motion in a data-driven form, by constructing a "local connection model"—which is, in these systems, the dominant term of the reconstruction equation formulation of their Lagrangian mechanics [13–16]. The surprising success of this data-driven model [13], which assumed a viscous friction interaction with the ground instead of the expected Coulomb friction, prompted us to seek precise measurements of the actual contact forces involved in the motions we studied. We aimed to understand what interactions contributed to the unexpectedly good predictive power of the "wrong" friction model.

We built a version of the BigANT robot [17] with a 6-DoF F/T transducer at the hip of each leg. This, we believed, would enable us to measure the wrench applied by each leg to the robot chassis, and since the shape of the leg and its point of contact were known from motion tracking, to compute the contact force that produced each leg's wrench. We chose to install the F/T transducers at the hips, mounted directly on the robot's chassis to maintain the lightweight, fast-swinging nature of the legs. Additionally, the commercial transducers we found for the range of wrenches expected were both heavy and fragile to impact, making it infeasible to attach them directly to the tip of a foot. The wrench each transducer measured comprises the ground contact wrench, added to the wrench generated by gravity acting on the (albeit lightweight) leg. Our calibration procedure needed to decouple these two terms to isolate the ground reaction wrench we wanted to measure.

Few have measured multilegged contact wrenches simultaneously at all active contacts. One example is in Ref. [18] wherein the authors measured three-dimensional (3D) ground reaction forces for a version of the hexapod RHex. The authors did not provide details on characterization and analysis of measurement error, but did provide 2 N as the maximum error. The authors of Ref. [19] performed in situ calibration with F/T transducers mounted on the shoulders, hips, and feet of a bipedal robot. They used the model from their computer aided manufacturing design file to extract the center of mass (CoM) of each segment and estimate the torque resulting from the gravity of each segment.

Below, we present a calibration procedure enabling simultaneous measurement of all foot contact wrenches of our multilegged robot using six 6-DoF F/T transducers, one at the hip of each leg. We start with introducing the experimental setup in Sec. 2.1, followed by

[1]Corresponding author.

Contributed by the Dynamic Systems Division of ASME for publication in the Journal of Dynamic Systems, Measurement, and Control. Manuscript received January 22, 2024; final manuscript received August 18, 2024; published online September 30, 2024. Assoc. Editor: Gregory Buckner.

difficulties we met when using the transducers naively according to the manufacturer's guidelines in Sec. 2.2. We present the problem statement including notations and F/T measurement model in this calibration work in Sec. 3, and follow with our calibration method in Sec. 4. We then show our validation of the calibration results in Sec. 5 and end with a discussion in Sec. 6.

2 Calibration Challenges

2.1 Experimental System: Robot and Sensors. Our goal was to measure the ground contact wrenches with respect to a "floating base" frame attached to the robot chassis. The robot we used was a version of the BigANT hexapod [17] (Fig. 1) constructed using plate and reinforced flexure methodology [11]. The z axis of the frame was opposite to the direction of gravity, and the x axis was perpendicular to the z and parallel to the left-right symmetry axis of the robot. The origin of the floating base frame was taken to be close to the centroid of the robot chassis.

Because of all the instrumentation planned for this robot, it was far heavier than previous BigANT variants. To ensure better rigidity under these loads in comparison to other BigANT variants we used a 1/4 inch acrylonitrile butadiene styrene sheet for the chassis baseplate. Connecting each leg to the robot chassis, we installed an ATI Industrial Automation Net Force/Torque Gamma transducer, which measured all six components of force and torque at 100 Hz and reported the results over WiFi. As in other BigANT robots, we actuated each leg with a position controlling servomotor module (Robotis Dynamixel MX106). We daisy-chained the modules as they were designed to be used, and communicated with them over the RS-485 serial bus carried over two wires of this daisy chain. The total weight of the robot was 8.18 kg, measured by a digital hanging scale. Along with the F/T data, we also recorded robot kinematic data using a reflective marker motion tracking system (10 Qualisys Oqus-310+ cameras at 100 fps, 12 markers on the chassis, and 4 markers per the distal rigid part of each leg).

Each leg of BigANT is driven by a four-bar mechanism producing a shaped toe trajectory (Fig. 1) with a variable gearing ratio. Because the legs were effectively rigid 1-DoF mechanisms (as verified using motion tracking), the shape of each leg changed through a one-parameter family of shapes entirely controlled by the shaft angle of the motor driving that leg. Consequently, the location of the CoM of each leg (with respect to the chassis frame) was also solely a function of that leg's shaft angle. Therefore, the gravity torque introduced by each leg on its hip F/T transducer was a function of the direction of gravity in the chassis frame (shared among legs), and the shaft angle of the individual leg.

2.2 Pre-Experimental Force/Torque Transducer Measurement Validations. As a sanity check prior to collecting motion data, we collected measurements with the robot standing statically at different poses. Because acceleration is zero, the total wrench on the robot body should be equal and opposite to gravity acting on the robot body through the body's CoM, i.e., when accounting for gravity, the sum of forces on the robot body should be zero. The ATI user's manual [20] suggests that the transducers may suffer from a constant bias wrench which needs to be subtracted. We used the average transducer readings obtained with all feet in the air rotating two full cycles as this constant bias term for each transducer. The

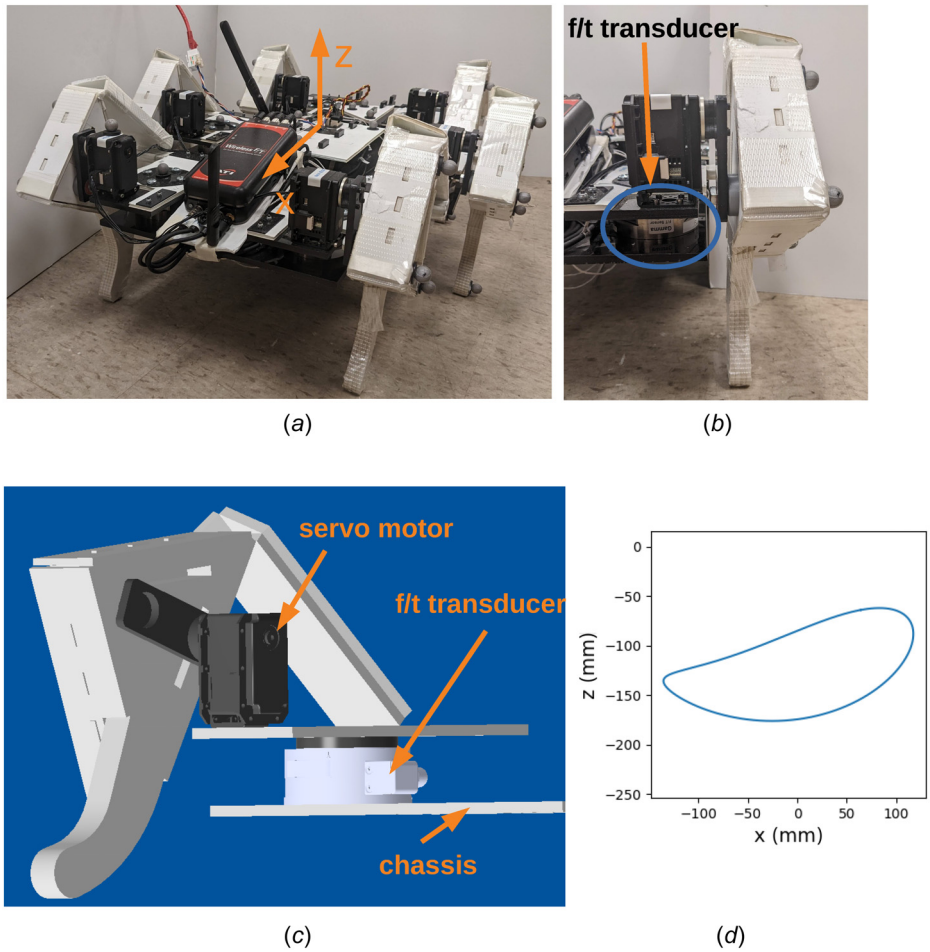

(*a*) (*b*) (*c*) (*d*)

Fig. 1 (*a*) BigANT equipped with six 6-axis force/torque transducers, (*b*) zoomed-in view of one leg with F/T transducers, (*c*) schematic drawing of front right leg module, and (*d*) 1-DoF toe tip trajectory in robot body frame xz-plane

total wrench applied to the body by the legs under these conditions had a standard deviation of approximately 5 N, and the force was distributed from—5 N to 20 N, shown in Fig. 2—nowhere near the expected gravitational wrench.

We collected F/T measurements and motion tracking data with BigANT standing at different poses. We positioned the robot in all $3^6 = 729$ combinations of three shaft angle possibilities for each leg: 0 deg (pointing straight down) or ± 36 deg. We waited for 5 s between consecutive poses. When a pose transitioned to the next pose, we observed that both the wrench and motion tracking measurements exhibited an overshooting oscillatory behavior. We estimated the first order derivative of both data streams using a second order `scipy.signal.savgol_®lter` filter in Python. We considered a pose to have reached a steady-state if the L2-norm of this numerical differentiation on force data decayed to less than 1 N/s. If a pose stayed at this "steady-state" for more than 1.5 s, we took the median of the steady-state measurements to represent this pose, thereby using the median filter's superior outlier rejection to guard against any nonzero mean noise processes. If a pose did not reach a "steady-state," we discarded that pose; this process left us with recordings from 635 poses. We further discarded those poses that did not have all 12 markers on the chassis tracked by the motion capture system, leaving us with 543 poses. We transformed the transducer measurements from the transducer frame into the floating base frame, where frame transformations were estimated by solving the orthogonal Procrustes problem using singular value decomposition on the 12 chassis markers.

The transducers themselves were precalibrated by ATI, and used in their normal operating region. The nonphysical total body wrenches we obtained lead us to conclude that more a complete calibration procedure may be advisable for improving the accuracy of these measurements.

2.3 Background on Force/Torque Transducer Calibration. ATI, the transducer manufacturer, instructs that we should expect an offset error for the transducers, i.e., that a nonzero reading should appear even when the transducer is unloaded and that this reading is added to all measurements made by that transducer. The ATI recommendation is for users to mechanically disconnect all transducers and recalibrate them periodically. While this calibration could remove such an expected transducer offset, removing and reinstalling the transducers could introduce a different assembly error every time. Also, a fixed offset error cannot account for the variable gravity force of a leg as it is moving through various positions. Hence, we decided to design an in situ calibration procedure.

A common method to perform in situ calibration of F/T transducers in robotic manipulators is to attach a test mass to the transducer, and then take several measurements with the transducer at different orientations. Using the fact that the external force applied to the transducer – the gravity of the attached mass – is fixed in the world frame, one can use least squares methods to estimate calibration parameters. The authors of Refs. [3,21] solved for an in situ calibration matrix, which transformed strain gauge values to forces and torques. The authors of Ref. [22] solved for in situ calibration matrix together with a rotation matrix between the world frame and the robot base frame, to account for the error caused by a tilted robot base of a manipulator. The authors of Ref. [23] did gravity compensation for a tool together with estimating the transformation matrix between the transducer frame and the robot frame. All of these researchers attached their F/T transducer rigidly fixed with respect to the end effector being loaded with the test mass.

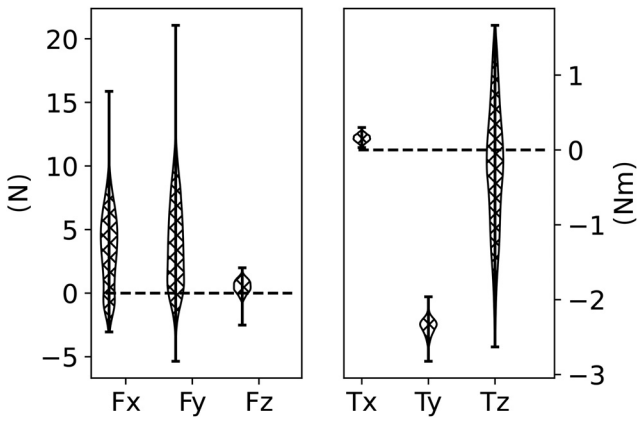

Fig. 2 Violin plot of the sum of all wrenches acting on the robot when standing at 543 different poses, corresponding to various combinations of each leg motor shaft at 0, +36°, and −36°. As the wrench measurement in each (static) pose we used the median of each of the wrench components over the same 1.5 s time interval, collected at 100 samples per second. To ensure no transient motions contaminate this static-by-design measurement, we only used poses where we could find such a time interval with the *L2* norm of the derivative of all force components (computed with a second order Savitsky-Golay filter, 11 sample window) below 1 *N*/*s*. For the measurements themselves, we used the calibration procedure suggested by the vendor, consisting of constant offset removal. See body text for additional details.

2.4 Leg Shape Changes Provide a Challenge. In our robot, the CoM of each leg was not at a constant location in the body frame, but instead moved as a function of its drive shaft angle. We also observed that our placement of the transducers was not perfectly aligned and precise relative to the robot body frame, i.e., there were sometimes mounting position and orientation errors. Furthermore, the origin of the robot body frame was not the CoM of the robot body—only close to it. It is practically quite difficult to precisely estimate the CoM of a robot built and assembled with parts using many kinds of materials, and even with light legs, this CoM will shift as the legs move.

The in situ calibration procedures available in the robotic manipulation literature could assume near-perfect positioning of the test mass by controlling the robot joints. The only reorientation available to us was to hang the robot from various attachment points to change the transducer frame orientations with respect to gravity. However, this hanging angle was itself difficult to measure in the body frame. Below, we present a calibration procedure that addresses all of the aforementioned challenges.

Besides these error sources, we also discovered that the transducer casing was not well isolated from forces applied to the exterior of this seemingly rigid metal casing. As an illustration of these issues, we wrapped 1–7 rubber bands (OfficeMax size 16) around the sensor case of an unloaded sensor. The transducer's measurements in the xy-axis changed by as much as 1 N. By gently pulling one rubber band to create a nonuniform load around the case, the readings from the transducer xy-axis changed by 3 N.

3 Force/Torque Sensing Model

In this section, we present our notation, sensor model, and calibration parameters. We use bold upper-case letters to represent matrices (e.g., $\mathbf{T}, \mathbf{R}$); and bold lower-case letters to represent vectors (e.g., $\mathbf{w}, \mathbf{r}$). We use the generalized force, wrench $\mathbf{w} = [\mathbf{f}; \boldsymbol{\tau}]^\mathsf{T}$, to represent linear components (forces $\mathbf{f} \in \mathbb{R}^3$) and angular components (torques $\boldsymbol{\tau} \in \mathbb{R}^3$). We use '; ' to separate elements in column vectors, and ', ' to separate elements in row vectors. We use $\mathbf{T}_\mathsf{A}^\mathsf{B}$ to represent rigid-body motion $\mathbf{SE}(3)$ from frame A to frame B. The homogeneous transformation representation is

$$\mathbf{T}_\mathsf{A}^\mathsf{B} = \begin{bmatrix} \mathbf{R}_\mathsf{A}^\mathsf{B} & \mathbf{p}_\mathsf{A}^\mathsf{B} \\ \mathbf{0} & 1 \end{bmatrix} \in \mathbb{R}^{4\times 4}$$

Here, $\mathbf{R}_\mathsf{A}^\mathsf{B} \in \mathrm{SO}(3)$ is the rotation from frame A to B, and $\mathbf{p}_\mathsf{A}^\mathsf{B} \in \mathbb{R}^3$ is the translation from the origin of A to the origin of B. By abuse of

notation, we omit 1 in the homogeneous transformation in the later calculations, i.e., $\mathbf{r}^{\mathsf{A}} \in \mathbb{R}^3$, $\mathbf{T}^{\mathsf{B}}_{\mathsf{A}}\mathbf{r}^{\mathsf{A}} := \mathbf{T}^{\mathsf{B}}_{\mathsf{A}}[\mathbf{r}^{\mathsf{A}}; 1] = [\mathbf{r}^{\mathsf{B}}; 1] =: \mathbf{r}^{\mathsf{B}}$. We transform wrenches from frame A to frame B via the transposed adjoint of $\mathbf{T}^{\mathsf{A}}_{\mathsf{B}}$

$$\mathbf{w}^{\mathsf{B}} = [\mathrm{Ad}_{\mathbf{T}^{\mathsf{A}}_{\mathsf{B}}}]^{\mathsf{T}}\mathbf{w}^{\mathsf{A}}$$

$$\begin{bmatrix}\mathbf{f}^{\mathsf{B}}\\ \boldsymbol{\tau}^{\mathsf{B}}\end{bmatrix} = \begin{bmatrix}(\mathbf{R}^{\mathsf{A}}_{\mathsf{B}})^{\mathsf{T}} & \mathbf{0}\\ -(\mathbf{R}^{\mathsf{A}}_{\mathsf{B}})^{\mathsf{T}}[\mathbf{p}^{\mathsf{A}}_{\mathsf{B}}] & (\mathbf{R}^{\mathsf{A}}_{\mathsf{B}})^{\mathsf{T}}\end{bmatrix}\begin{bmatrix}\mathbf{f}^{\mathsf{A}}\\ \boldsymbol{\tau}^{\mathsf{A}}\end{bmatrix}$$

where the notation $[\mathbf{p}^{\mathsf{B}}_{\mathsf{A}}]$ lifts the 3d vector $\mathbf{p}^{\mathsf{B}}_{\mathsf{A}}$ to a skew symmetric matrix. The frame of reference for a value of interest is on the upper right corner. We use k to denote the index of the legs, i.e., wrench w. r.t. frame A on leg k is $\mathbf{w}^{\mathsf{A}}_{\mathsf{k}}$.

The coordinate frames of interest are B: robot body frame; C: robot body frame centered at the true CoM; W: floating base frame; ft_{k}: F/T transducer frame of the kth leg. We use $\mathbf{g} = [0, 0, g]$ to represent the gravitational acceleration in the floating base frame.

We use ϕ to represent the shaft angle governing the shape of the four-bar linkage leg, m to represent the mass of a leg, and $\mathbf{r}(\phi)$ to represent the leg CoM as a function of ϕ. We use $i = 1, \ldots, N$ to denote the index for the time series. We use a superscript asterisk $\square^*$ to denote the optimal value of a variable in an optimization. In Sec. 4.1, where we hang the robot, we use $\square^{\downarrow}$ and $\square^{\uparrow}$ to denote a value associated with positive and negative hanging direction. We use $\square^- =: (\square^{\downarrow} - \square^{\uparrow})/2$ and $\square^+ =: (\square^{\downarrow} + \square^{\uparrow})/2$ to denote anti-symmetric and symmetric parts of a value with respect to opposite hanging directions.

3.1 Sensor Model. From our experiments, we noticed that for each transducer there existed a constant offset, independent of load, which was also mentioned in ATI F/T transducer manual [20]. We modeled the measured wrench $\mathbf{w}^{\mathrm{ft}_{\mathsf{k}}}_{m}$ by the kth force/torque transducer as the sum of the applied wrench $\mathbf{w}^{\mathrm{ft}_{\mathsf{k}}}_{a}$, an unknown transducer offset $\mathbf{w}^{\mathrm{ft}_{\mathsf{k}}}_{o} \in \mathbb{R}^6$ and random noise $\mathbf{n}$

$$\mathbf{w}^{\mathrm{ft}_{\mathsf{k}}}_{m} =: \mathbf{w}^{\mathrm{ft}_{\mathsf{k}}}_{a} + \mathbf{w}^{\mathrm{ft}_{\mathsf{k}}}_{o} + \mathbf{n} \tag{1}$$

Since the transducers were installed underneath the legs, when a leg was in the swinging phase (not contacting the ground), the wrench resulting from the leg gravity was applied to the transducer. We decomposed the applied wrench $\mathbf{w}^{\mathrm{ft}_{\mathsf{k}}}_{a}$ into two parts: the wrench resulted from the gravity of kth leg and the ground contact wrench. The shaft angle ϕ_{k} governed the shape of the four-bar linkage of each leg, and hence changed its CoM. We modeled the kth leg CoM position in the transducer frame by $\mathbf{r}^{\mathrm{ft}_{\mathsf{k}}}_{\mathsf{k}}(\phi_{\mathsf{k}})$. We used leg gravitational offset $\mathbf{w}^{\mathsf{W}}_{\mathrm{leg},\mathsf{k}}(\phi_{\mathsf{k}})$, a function of ϕ_{k}, to represent the wrench gravity applied to the leg with respect to the transducer. The gravitational acceleration is constant in the floating base frame. We transformed the leg CoM position in the transducer frame to the floating base frame, allowing us to write the leg gravitational offset wrench

$$\mathbf{w}^{\mathsf{W}}_{\mathrm{leg},\mathsf{k}}(\phi_{\mathsf{k}}) =: [m_k\mathbf{g}; \mathbf{T}^{\mathsf{W}}_{\mathrm{ft}_{\mathsf{k}}}\mathbf{r}^{\mathrm{ft}_{\mathsf{k}}}_{\mathsf{k}}(\phi_{\mathsf{k}}) \times m_k\mathbf{g}]$$

We decomposed the transformation from the kth F/T transducer to the floating base frame in four steps

$$\mathbf{T}^{\mathsf{W}}_{\mathrm{ft}_{\mathsf{k}}} =: \mathbf{T}^{\mathsf{W}}_{\mathsf{C}}\mathbf{T}^{\mathsf{C}}_{\mathrm{ft}_{\mathsf{k}}} = \mathbf{T}^{\mathsf{W}}_{\mathsf{C}}\mathbf{T}^{\mathsf{C}}_{\mathsf{B}}\tilde{\mathbf{T}}_k\mathbf{T}^{\mathsf{B}}_{\mathrm{ft}_{\mathsf{k}}} \tag{2}$$

(1) a nominal transformation, $\mathbf{T}^{\mathsf{B}}_{\mathrm{ft}_{\mathsf{k}}}$, from the kth transducer frame to the body frame, calculated from robot design files;
(2) unknown transformation $\mathbf{T}_k$ to compensate for the installation or manufacturing error, which was not captured by step 1;
(3) unknown translation $\mathbf{T}^{\mathsf{C}}_{\mathsf{B}}$ between the origin of the body frame and robot CoM.
(4) a pure rotation $\mathbf{T}^{\mathsf{W}}_{\mathsf{C}}$ estimated from markers measured by the motion tracking system, rotating the body frame centered at CoM into the floating base frame.

Let $\mathbf{g}^{\mathsf{C}} = \mathbf{R}^{\mathsf{C}}_{\mathsf{W}}\mathbf{g}$ be the gravitational acceleration rotated into the body CoM frame. We used $\mathbf{w}^{\mathsf{C}}_{\mathrm{gc},k}(\phi_{\mathsf{k}})$ to denote the ground contact wrench in the body CoM frame, calculated from the applied wrench $\mathbf{w}^{\mathrm{ft}_{\mathsf{k}}}_{a}$ transformed in the CoM frame and subtracted by the wrench from leg gravity

$$\begin{aligned}
\mathbf{w}^{\mathsf{C}}_{\mathrm{gc},k}(\phi_{\mathsf{k}}, \mathbf{g}^{\mathsf{C}}) &=: [\mathrm{Ad}_{(\mathbf{T}^{\mathsf{C}}_{\mathrm{ft}_{\mathsf{k}}})^{-1}}]^{\mathsf{T}}\mathbf{w}^{\mathrm{ft}_{\mathsf{k}}}_{a} - \mathbf{w}^{\mathsf{C}}_{\mathrm{leg},\mathsf{k}}(\phi_{\mathsf{k}}, \mathbf{g}^{\mathsf{C}})\\
(\text{substitute } \mathbf{T}^{\mathrm{ft}_{\mathsf{k}}}_{\mathsf{C}} \text{ by eqn.2}) &= [\mathrm{Ad}_{(\mathbf{T}^{\mathsf{C}}_{\mathsf{B}}\tilde{\mathbf{T}}_k\mathbf{T}^{\mathsf{B}}_{\mathrm{ft}_{\mathsf{k}}})^{-1}}]^{\mathsf{T}}\mathbf{w}^{\mathrm{ft}_{\mathsf{k}}}_{a} - \mathbf{w}^{\mathsf{C}}_{\mathrm{leg},\mathsf{k}}(\phi_{\mathsf{k}}, \mathbf{g}^{\mathsf{C}})\\
(\text{substitute } \mathbf{w}^{\mathrm{ft}_{\mathsf{k}}}_{a} \text{ by eqn.1}) &= [\mathrm{Ad}_{(\mathbf{T}^{\mathsf{C}}_{\mathsf{B}}\tilde{\mathbf{T}}_k\mathbf{T}^{\mathsf{B}}_{\mathrm{ft}_{\mathsf{k}}})^{-1}}]^{\mathsf{T}}(\mathbf{w}^{\mathrm{ft}_{\mathsf{k}}}_{m} - \underline{\mathbf{w}^{\mathrm{ft}_{\mathsf{k}}}_{o}})\\
(\text{rewrite } \mathbf{w}^{\mathrm{ft}_{\mathsf{k}}}_{o} \text{ in f/t elements}) &- [\underline{m_k\mathbf{g}^{\mathsf{C}}}; \underline{\mathbf{T}^{\mathsf{C}}_{\mathsf{B}}\tilde{\mathbf{T}}_k\mathbf{T}^{\mathsf{B}}_{\mathrm{ft}_{\mathsf{k}}}}\mathbf{r}^{\mathrm{ft}_{\mathsf{k}}}_{\mathsf{k}}(\phi_{\mathsf{k}}) \times \underline{m_k\mathbf{g}^{\mathsf{C}}}]
\end{aligned} \tag{3}$$

We transformed this wrench into the floating base frame using the motion tracking rotation $[\mathrm{Ad}_{\mathbf{T}^{\mathsf{C}}_{\mathsf{W}}}]^T$. All the unknown calibration parameters are underlined in Eq. (3). In the remainder of this paper, leg CoM $\mathbf{r}_{\mathsf{k}}(\phi_{\mathsf{k}})$ was always considered to be in the transducer ft_{k} frame, and associated with the k^{th} shaft angle. We therefore omitted ft_{k} the leg CoM and k in ϕ_k, as $\mathbf{r}_{\mathsf{k}}(\phi)$ to simplify the notation.

4 Calibration Method

In this section, we documented our method to infer parameters by using several optimizations applied to measurement data. We formulated our parameter estimation goal function by using the fact that the force of gravity on the robot and its legs must be constant in the floating base frame. Our calibration had two steps: (1) we estimated the transducer offset $\mathbf{w}^{\mathrm{ft}_{\mathsf{k}}}_{o}$ and leg gravity offset $\mathbf{w}^{\mathsf{W}}_{\mathrm{leg},\mathsf{k}}$, by summing up the measurements with leg gravity acting in opposite directions in the transducer frame. Because perfectly opposite measurements were never possible in reality, we assumed the existence of a small rotational term that could leak m_kg into the other two directions, and bias the estimation of offsets. We modeled this small rotation error as the identity plus a small skew-symmetric matrix, and solved for the 3D skew part together with other parameters. (2) we estimated the transformation error together with the unknown translation between body frame origin and CoM $\mathbf{T}^{\mathsf{C}}_{\mathsf{B}}\tilde{\mathbf{T}}_k$, by having the robot standing at different poses, then optimizing the error between the sum of all ground contact wrenches in the floating frame and $[0, 0, G_{\mathrm{robot}}, 0, 0, 0]^T$, namely, the robot gravity with zero total torque.

4.1 Transducer Offset and Leg Gravity Offset. To model the wrench applied by gravity to a leg with respect to its transducer, we estimated the leg CoM as a function of shaft angle. Because this measurement is influenced by the transducer offset, we estimated the CoM function of the shaft angle together with the transducer offset. We collected measurements with the robot hanging (zero ground contact wrenches) in opposite directions, while at the same time slowly (quasi-statically) rotating each leg ten full cycles with 9000 sample points for each cycle (see, e.g., opposite z-directions in Fig. 3). The torque that resulted from leg gravity arises from a cross-product with leg CoM, leaving a one-dimension null space when estimating from each pair of hanging experiments (more details in Sec. 4.1.3). To get a complete 3D CoM function of shaft angle, we repeated the procedure twice: two pairs of opposite orientations, one along the transducer $\pm x$-axis, and one along the transducer $\pm z$-axis (aligning with gravity).

In the rest of this section, we used the experiments of transducer $\pm x$-axis aligning with gravity to explain the calculation; the calculation with z-axis positive or negative direction aligning with gravity could be performed analogously.

4.1.1 Hanging Measurement Model. We considered a measurement model using a skew-symmetric matrix $[\mathbf{s}_{\mathsf{k}}]$, lifted from

$\mathbf{s}_k \in \mathbb{R}^3$, to model the axis misalignment error between the direction of gravity and the transducer axis. We assumed $\mathbf{s}_k$ was constant throughout one time series, i.e., the transducer orientation did not change throughout the measurement. The skew-symmetric matrix $[\mathbf{s}_k]$, the tangent space at identity rotation, could be viewed as an infinitesimally small rotation in the form of $[\mathbf{s}_k] + \mathbf{I}$. The applied wrench, when leg gravity aligned with the positive x-axis of the transducer frame, became

$$\mathbf{f}_a^{\mathrm{ft_k},\downarrow} = ([\mathbf{s}_k^{\downarrow}] + \mathbf{I}) m_k \mathbf{g}_x$$
$$\boldsymbol{\tau}_a^{\mathrm{ft_k},\downarrow} = [\mathbf{r}_k(\phi)]([\mathbf{s}_k^{\downarrow}] + \mathbf{I}) m_k \mathbf{g}_x$$

Its opposite applied wrench, when leg gravity aligned with negative x-axis of the transducer frame, was the same magnitude with opposite direction

$$\mathbf{f}_a^{\mathrm{ft_k},\uparrow} = -([\mathbf{s}_k^{\uparrow}] + \mathbf{I}) m_k \mathbf{g}_x$$
$$\boldsymbol{\tau}_a^{\mathrm{ft_k},\uparrow} = -[\mathbf{r}_k(\phi)]([\mathbf{s}_k^{\uparrow}] + \mathbf{I}) m_k \mathbf{g}_x$$

Here $[\mathbf{s}_k^{\downarrow}]$ and $[\mathbf{s}_k^{\uparrow}]$ were two skew-symmetric matrices, accounting for two different small rotations between F/T transducer positive or negative x-axis and world z-axis. During the experiment, we measured F/T data for both of these two configurations, with the same set of varying shaft angles ϕ_i, for $i = 1, \ldots, N$, covering the full range of motion multiple times. We modeled the measured wrenches, according to Eq. (1), and partitioned them into their force and torque components in Eqs. (4)–(7), where $\boldsymbol{v}_i^{\downarrow}, \boldsymbol{v}_i^{\uparrow}, \boldsymbol{\omega}_i^{\downarrow}, \boldsymbol{\omega}_i^{\uparrow}$ were realization of random noise for the ith measurement

$$\mathbf{f}_{m,i}^{\mathrm{ft_k},\downarrow} = ([\mathbf{s}_k^{\downarrow}] + \mathbf{I}) m_k \mathbf{g}_x + \mathbf{f}_o^{\mathrm{ft_k}} + \boldsymbol{v}_i^{\downarrow} \tag{4}$$

$$\mathbf{f}_{m,i}^{\mathrm{ft_k},\uparrow} = -([\mathbf{s}_k^{\uparrow}] + \mathbf{I}) m_k \mathbf{g}_x + \mathbf{f}_o^{\mathrm{ft_k}} + \boldsymbol{v}_i^{\uparrow} \tag{5}$$

$$\boldsymbol{\tau}_{m,i}^{\mathrm{ft_k},\downarrow} = [\mathbf{r}_k(\phi_i)]([\mathbf{s}_k^{\downarrow}] + \mathbf{I}) m_k \mathbf{g}_x + \boldsymbol{\tau}_o^{\mathrm{ft_k}} + \boldsymbol{\omega}_i^{\downarrow} \tag{6}$$

$$\boldsymbol{\tau}_{m,i}^{\mathrm{ft_k},\uparrow} = -[\mathbf{r}_k(\phi_i)]([\mathbf{s}_k^{\uparrow}] + \mathbf{I}) m_k \mathbf{g}_x + \boldsymbol{\tau}_o^{\mathrm{ft_k}} + \boldsymbol{\omega}_i^{\uparrow} \tag{7}$$

4.1.2 Leg Gravity, $m_k\mathbf{g}$. We subtracted two opposite force measurements between Eqs. (4) and (5). By dividing the difference by 2, we got the leg gravity multiplied by a small rotation error term in the front

$$\frac{(4)-(5)}{2}: \quad \mathbf{f}_{m,i}^{\mathrm{ft_k},-} = \left(\frac{[\mathbf{s}_k^{\downarrow}]+[\mathbf{s}_k^{\uparrow}]}{2} + \mathbf{I}\right) m_k \mathbf{g}_x + \frac{\boldsymbol{v}_i^{\downarrow} - \boldsymbol{v}_i^{\uparrow}}{2}$$

The sum of two skew-symmetric matrices is still skew-symmetric, denoted by $[\mathbf{s}_k^{+}] = ([\mathbf{s}_k^{\downarrow}] + [\mathbf{s}_k^{\uparrow}])/2$. Ideally, $m_k\mathbf{g}_x$ was equal to $[m_k g, 0, 0]$, a constant value in x component, and zeros in y, z components. Taking that as the optimization goal, with N measurement samples $\mathbf{f}_{m,i}^{\mathrm{ft_k},-}$ for $i = 1, \ldots, N$, we solved for $\mathbf{s}_k^{+}$ using `scipy.optimize.least_squares` with the Trust Region Reflective algorithm and cost function tolerance 10^{-3}

$$\mathbf{s}_k^{+,*} = \arg\min_{\mathbf{s}_k^{+}} \frac{1}{\sqrt{N}} \sum_{j=2,3} \sqrt{\sum_{i=1}^{N} \left(\left([\mathbf{s}_k^{+}] + \mathbf{I} \right)^{-1} \mathbf{f}_{m,i}^{\mathrm{ft_k},-} \cdot \mathbf{e}_j \right)^2 + \mathrm{std}_{i=1,\ldots,N} \left(\left([\mathbf{s}_k^{+}] + \mathbf{I} \right)^{-1} \mathbf{f}_{m,i}^{\mathrm{ft_k},-} \cdot \mathbf{e}_1 \right)}$$

where, $\mathbf{e}_j$ with $j = 1, 2, 3$ are unit vectors in $\mathbb{R}^3$. We estimated the gravity of the leg by

$$m_k g = 1/N \sum_{i=1}^{N} (([\mathbf{s}_k^{+,*}] + \mathbf{I})^{-1} \tilde{\mathbf{f}}_{m,i}^{\mathrm{ft_k}} \cdot \mathbf{e}_1)$$

4.1.3 Leg Center of Mass, $\mathbf{r}_k(\phi)$. Next, we solved for the leg CoM by subtracting Eqs. (6) and (7)

$$\frac{(6)-(7)}{2}: \quad \boldsymbol{\tau}_{m,i}^{\mathrm{ft_k},-} = [\mathbf{r}_k(\phi_i)]\left([\mathbf{s}_k^{+}] + \mathbf{I}\right) m_k \mathbf{g}_x + \boldsymbol{\omega}_i^{-} = [\mathbf{r}_k(\phi_i)] \mathbf{f}_{m,i}^{\mathrm{ft_k},-} + \boldsymbol{\omega}_i^{-}$$

Here, $\boldsymbol{\tau}_{m,i}^{\mathrm{ft_k},-}$ and $\mathbf{f}_{m,i}^{\mathrm{ft_k},-}$ could be calculated directly from the measurement data. We estimated the leg CoM $\mathbf{r}_{\mathrm{est,k}}(\phi)$ as a function of ϕ through a Kalman smoother [24], after obtaining N samples measured with varying shaft angle ϕ_i, $i = 1, \ldots, N$. We set the transition and observation covariance matrices in the Kalman smoother both having 0.01 on the diagonal and 0 on the off-diagonal elements, which matched the magnitude of the measured covariance. Since the torque was the cross product between the CoM vector and gravity, the estimated CoM here had a one-dimensional null space along the direction of $\tilde{\mathbf{f}}_{m,i}^{\mathrm{ft_k}}$. The CoM could be $\mathbf{r}_k(\phi_i) = \mathbf{r}_{\mathrm{est,k}}(\phi_i) + p_i \cdot \tilde{\mathbf{f}}_{m,i}^{\mathrm{ft_k}}$, for any scalar $p_i \in \mathbb{R}$. Therefore, we needed at least another pair of opposite hanging measurements to get full rank information on $\mathbf{r}_k(\phi)$. In our experiment, we took measurements with leg gravity aligning with the $\pm z$-axis of the transducer frame and performed analogous calculations mentioned above with $\mathbf{g}_z$. We obtained another estimation $\mathbf{r}'_{\mathrm{est,k}}(\phi)$ where $\mathbf{r}_k(\phi_i) = \mathbf{r}'_{\mathrm{est,k}}(\phi_i) + p'_i \cdot \tilde{\mathbf{f}}'^{\mathrm{ft_k}}_{m,i}$. We solved p_i, p'_i by equating two $\mathbf{r}_k(\phi)$ obtained from two sets of measurements. This formed an over-determined system with three equations and two unknowns which we solved for the unknowns p_i, p'_i by ordinary least squares. We averaged those two $\mathbf{r}_k$ and fit a function with respect to ϕ.

4.1.4 Transducer Offset, $\mathbf{w}_o^{ft_k} = [\mathbf{f}_o^{ft_k}; \boldsymbol{\tau}_o^{ft_k}]$. We solved for transducer torque offset $\boldsymbol{\tau}_o^{\mathrm{ft_k}}$, by adding Eqs. (6) and (7)

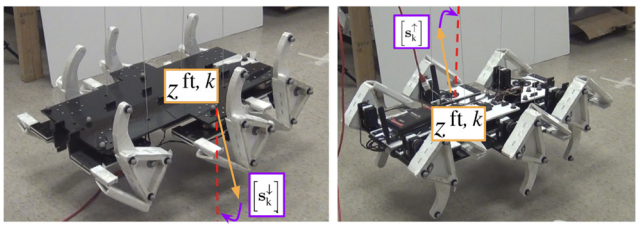

Fig. 3 BigAnt robot hanging with transducer z-axis positive $z^{\mathrm{ft_k}}$ (orange) and negative direction aligning with gravity direction (red); $[\mathbf{s}_k^{\downarrow}]$ and $[\mathbf{s}_k^{\uparrow}]$ (purple): skew symmetric matrices modeling the hanging orientation error

$$\frac{(6)+(7)}{2}: \quad \boldsymbol{\tau}_{m,i}^{\mathrm{ft_k},+} = [\mathbf{r}_{\mathsf{k}}(\phi_i)]\left(\frac{\left[\mathbf{s}_{\mathsf{k}}^{\downarrow}\right]-\left[\mathbf{s}_{\mathsf{k}}^{\uparrow}\right]}{2}\right)m_k\mathbf{g}_x + \boldsymbol{\tau}_o^{\mathrm{ft_k}} + \frac{\boldsymbol{\omega}_i^{\downarrow}+\boldsymbol{\omega}_i^{\uparrow}}{2}$$

We denoted the subtraction between two skew symmetric matrices by $[\mathbf{s}_{\mathsf{k}}^{-}] = ([\mathbf{s}_{\mathsf{k}}^{\downarrow}] - [\mathbf{s}_{\mathsf{k}}^{\uparrow}])/2$. In the transducer model in Eq. (1), we assumed the transducer offset was constant. We solved for the optimal value of $\mathbf{s}_{\mathsf{k}}^{-}$ by minimizing the standard deviation of $\boldsymbol{\tau}_o^{\mathrm{ft_k}}$ over all samples

$$\mathbf{s}_{\mathsf{k}}^{-,*} = \arg\min_{\mathbf{s}_{\mathsf{k}}^{-}} \operatorname{std}_{i=1,\ldots,N}(\boldsymbol{\tau}_{m,i}^{\mathrm{ft_k},+} - [\mathbf{r}_{\mathsf{k}}(\phi_i)][\mathbf{s}_{\mathsf{k}}^{-}]m_k\mathbf{g}_x)$$

Finally, we calculated the force and torque offsets by

$$\mathbf{f}_o^{\mathrm{ft_k}} = \frac{1}{N}\sum_{i=1}^{N}\left(\frac{\mathbf{f}_{m,i}^{\mathrm{ft_k},\downarrow}+\mathbf{f}_{m,i}^{\mathrm{ft_k},\uparrow}}{2} - \left[\mathbf{s}_{\mathsf{k}}^{-,*}\right]m_k\mathbf{g}_x\right)$$
$$\boldsymbol{\tau}_o^{\mathrm{ft_k}} = \frac{1}{N}\sum_{i=1}^{N}\left(\boldsymbol{\tau}_{m,i}^{\mathrm{ft_k},+} - [\mathbf{r}_{\mathsf{k}}(\phi_i)]\left[\mathbf{s}_{\mathsf{k}}^{-,*}\right]m_k\mathbf{g}_x\right)$$

4.2 Transformation Error, $\mathbf{T}_{\mathsf{B}}^{\mathsf{C}}\tilde{\mathbf{T}}_k$. In the second part, we showed our method for estimating the transformation error from transducer frame to body frame, $\tilde{\mathbf{T}}_{\mathsf{k}}$ modeled by $(\tilde{\mathbf{R}}_{\mathsf{k}}, \tilde{\mathbf{p}}_{\mathsf{k}})$, together with an unknown transformation between body frame and CoM frame $\mathbf{T}_{\mathsf{B}}^{\mathsf{C}}$ modeled by $(\mathbf{I}_3, p_{\mathsf{B}}^{\mathsf{C}})$. We used the fact that the robot should be at force–torque balance when standing still at different poses. At each pose, the sum of the ground contact wrenches from all feet, transformed to the floating base frame, should equal to the gravity of the robot with zero torque, as calculated in Eq. (9). We used the same dataset as described in Sec. 2.2, and inferred the unknown parameters by minimizing the error between the total ground contact wrenches and the gravity of the robot with zero torque, as shown in Eq. (8). It minimized the difference between the measured and expected total wrench on CoM overall $p = 1, \ldots, P$ poses. The K-norm we used had a positive definite diagonal matrix $\mathbf{K}$ to allow us to compare loss functions computed over force and torque, which have different physical units. We used $\mathbf{K} := \mathrm{diag}([1,1,1,10,10,10])$ so the forces and torques had about the same numerical magnitude

$$\min_{\tilde{\mathbf{R}}_{\mathsf{k}},\tilde{\mathbf{p}}_{\mathsf{k}},\mathbf{p}_{\mathsf{B}}^{\mathsf{C}}} \sum_{p=1}^{P} ||(\mathbf{w}_{\mathrm{total},p}^{\mathsf{W}} - [0,0,G_{\mathrm{robot}},0,0,0]^T)||_{\mathbf{K}}^2 \quad \text{s.t.} \tilde{\mathbf{R}}_k \in \mathrm{SO}(3) \tag{8}$$

As formulated, the optimization problem needed to solve for the six rotation matrices $\tilde{\mathbf{R}}_{\mathsf{k}} \in \mathrm{SO}(3)$ is the 3D rotation group, which is not a vector space. However, most numerical optimization paradigms only work on vector spaces. Instead, we parameterized the rotation using Cayley transformation: $\tilde{\mathbf{R}}_{\mathsf{k}} = (\mathbf{I} - [\tilde{\mathbf{q}}_{\mathsf{k}}])(\mathbf{I} + [\tilde{\mathbf{q}}_{\mathsf{k}}])^{-1}$ [25]. This can represent rotation matrices over a wide range using a parameter space which is a vector space.

$$\begin{aligned}
\mathbf{w}_{\mathrm{total},p}^{\mathsf{W}} &= \sum_{k=1}^{K}[\mathsf{Ad}_{(\mathbf{T}_{\mathsf{C},p}^{\mathsf{W}})^{-1}}]^T\mathbf{w}_{\mathrm{gc},k}^{\mathsf{C}}(\phi_{p,\mathsf{k}}, \mathbf{g}_p^{\mathsf{C}}) \\
(\text{substitute } \mathbf{w}_{\mathrm{gc},k}^{\mathsf{C}} \text{ by eqn.3}) &= \sum_{k=1}^{K}[\mathsf{Ad}_{(\mathbf{T}_{\mathsf{C},p}^{\mathsf{W}})^{-1}}]^T(\mathsf{Ad}_{(\mathbf{T}_{\mathsf{B}}^{\mathsf{C}}\tilde{\mathbf{T}}_k\mathbf{T}_{\mathrm{ft_k}}^{\mathsf{B}})^{-1}}]^T(\mathbf{w}_{m,p}^{\mathrm{ft_k}} - \mathbf{w}_o^{\mathrm{ft_k}}) - [m_k\mathbf{g}_p^{\mathsf{C}}; \mathbf{T}_{\mathsf{B}}^{\mathsf{C}}\tilde{\mathbf{T}}_k\mathbf{T}_{\mathrm{ft_k}}^{\mathsf{B}}\mathbf{r}_{\mathsf{k}}^{\mathrm{ft_k}}(\phi_{p,\mathsf{k}}) \times m_k\mathbf{g}_p^{\mathsf{C}}]) \\
(\text{Expand } \mathbf{T}_{\mathsf{B}}^{\mathsf{C}}\tilde{T}_k) &= \sum_{k=1}^{K}\left(\begin{bmatrix}\mathbf{R}_{\mathsf{C}}^{\mathsf{W}} & \mathbf{0}\\ \mathbf{0} & \mathbf{R}_{\mathsf{C}}^{\mathsf{W}}\end{bmatrix}\begin{bmatrix}\tilde{\mathbf{R}}_k & \mathbf{0}\\ \tilde{\mathbf{R}}_{\mathsf{k}}[\tilde{\mathbf{R}}_k(\tilde{\mathbf{p}}_{\mathsf{k}} + \mathbf{p}_{\mathsf{B}}^{\mathsf{C}})] & \tilde{\mathbf{R}}_{\mathsf{k}}\end{bmatrix}[\mathsf{Ad}_{(\mathbf{T}_{\mathrm{ft_k}}^{\mathsf{B}})^{-1}}]^T(\mathbf{w}_{m,p}^{\mathrm{ft_k}} - \mathbf{w}_o^{\mathrm{ft_k}})\right. \\
&\quad \left. - \begin{bmatrix}m_k\mathbf{g};\begin{bmatrix}\mathbf{R}_{\mathsf{C}}^{\mathsf{W}} & \mathbf{0}\\ \mathbf{0} & 1\end{bmatrix}\begin{bmatrix}\tilde{\mathbf{R}}_k & \tilde{\mathbf{p}}_{\mathsf{k}} + \mathbf{p}_{\mathsf{B}}^{\mathsf{C}}\\ \mathbf{0} & 1\end{bmatrix}\mathbf{T}_{\mathrm{ft_k}}^{\mathsf{B}}\mathbf{r}_{\mathsf{k}}^{\mathrm{ft_k}}(\phi_{p,\mathsf{k}}) \times m_k\mathbf{g}\end{bmatrix}\right) \\
&\approx [0,0,G_{\mathrm{robot}},0,0,0]^T
\end{aligned} \tag{9}$$

From here, we made a change of variables $\tilde{\mathbf{p}}_k' = \tilde{\mathbf{R}}_k(\tilde{\mathbf{p}}_k + \mathbf{p}_{\mathsf{B}}^{\mathsf{C}})$. This made the objective function of the optimization Eq. (8) into a bilinear form in $\tilde{\mathbf{p}}_k'$ and $\tilde{\mathbf{R}}_{\mathsf{k}}$. To solve this optimization, we used dual least squares optimization, fixing one unknown and solving for the other, alternating which variable is fixed at each step, until it convergence. For each of these steps, we again used the `scipy.optimize.least_squares` Trust Region Reflective algorithm with cost function tolerance 10^{-3}. Our dual optimization convergence criterion was tested when the maximum norm difference between two successive steps was less than 10^{-3}.

5 Results

In this section, we report the estimated calibration parameters and the residual after calibration. We show the distribution of the residuals using violin plots. All violin plots used 100 points for the Gaussian kernel density estimation.

5.1 Transducer Offset and Leg Gravity Offset. The estimated transducer offset and the leg gravity were summarized in Supplemental Materials on the ASME Digital Collection. We plotted the estimated leg CoM trajectories on the midleft leg in Fig. 4 as an example. All the other legs had similar trajectories, as shown in Supplemental Materials. After removing the transducer offsets and the leg gravity offsets, we plotted the residual of all four measurement orientations in Fig. 5. We compared our formulation with the naive addition and subtraction that does not use the axis misalignment error $\hat{\mathbf{s}}$, modeling the imperfect hanging orientation.

5.2 Statistical Analysis on Wrench Transformation Error. We performed a model selection on 4 different models, to see the significance of the parameters used to model the wrench transformation error. We tested on

(1) The full model, fitting all six rotations ($\tilde{\mathbf{R}}_k$) and six translations ($\tilde{\mathbf{p}}_k'$), using $6 \times (3+3) = 36$ parameters;
(2) No transducer translation error ($\tilde{\mathbf{p}}_k = \mathbf{0}$), only fitting six rotations ($\tilde{\mathbf{R}}_k$) and one single unknown translation ($\mathbf{p}_{\mathsf{B}}^{\mathsf{C}}$) between robot center and CoM, using $6 \times 3 + 3 = 21$ parameters;

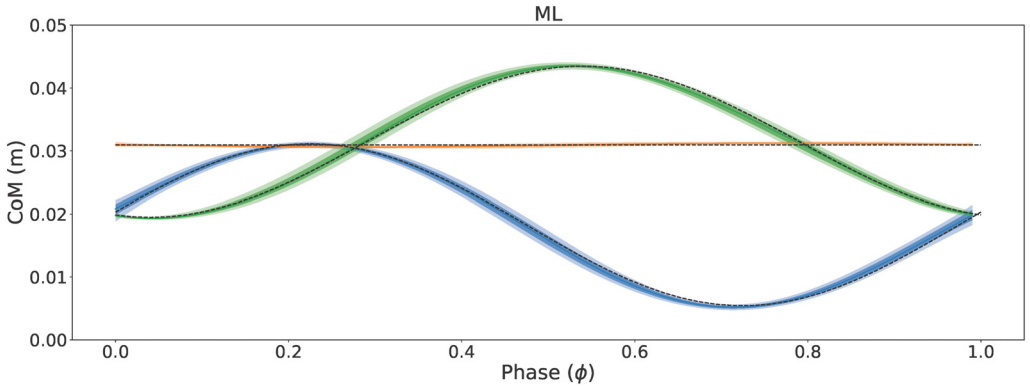

Fig. 4 Estimated center of mass (CoM) versus phase of Midleft (ML) leg. We plotted the median estimated CoM of ten cycles (solid line), interquartile range (dark shaded region), and 95% confidence interval (light shaded region; *x* coordinate in blue, *y* coordinate in orange, and *z* coordinate in green). We fitted the *x*, *z* coordinate with function $r(\phi) = A\sin(2\pi\phi + C) + D$, *y* coordinate using a constant (black dashes).

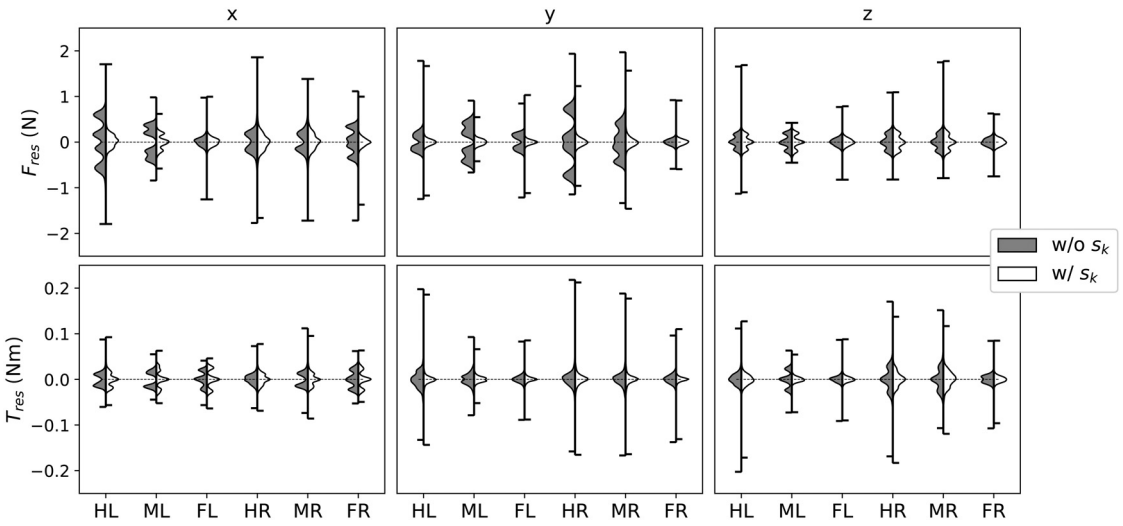

Fig. 5 Violin plot of force (first row) and torque (second row) residual on xyz-axis (columns) for all six transducers, with the skew symmetric matrices $\hat{\mathbf{s}}$ accounting for hanging orientation error (white filling), and without (gray filling). The measurements were collected with the robot hanging (zero ground contact wrenches) in $\pm x$, *z*-axis, while at the same time slowly (quasi-statically) rotating each leg ten full cycles with 9000 sample points for each cycle. (FL: front left, ML: midleft, HL: hind left, FR: front right, MR: midright, HR: hind right).

(3) No transducer rotation error ($\tilde{\mathbf{R}}_k = \mathbf{I}_3$), only fitting the transducer translation error together with robot center to CoM translation ($\tilde{\mathbf{p}}'_k$), using $6 \times 3 = 18$ parameters;
(4) With neither transducer rotation, nor translation error, only fitting a single unknown translation between robot center and CoM, using three parameters.

The statistics of those models are summarized in Table 1. We reported the mean of the mean squared error on 5-fold cross-validation, together with Bayesian information criterion $\text{BIC} = P\ln(\text{RSS}/P) + \text{DOF} \times \ln P$, where RSS is the residual sum squared. We selected (1) full model using six rotations and six translations, which yields the smallest Bayesian information criterion (BIC). We showed the residual plot comparing with and without transformation errors in Fig. 6.

Since the bilinear least-squares optimization only yielded local optima, we started the optimization process from 20 different randomized initial guesses within a plausible set, where the orientation error was less than 15 degrees in all three directions and the translation error was less than one-third of the robot size. The cost function variation was only 3.2% among all initial conditions.

5.3 Tripod Walking. We also collected the wrench and motion tracking data when the BigAnt robot used a tripod gait to walk quasi-statically. We generated the gait with a "Buehler clock," which provided a high shaft rotation speed during leg swing and a low shaft rotation speed while the leg was in stance, on an average running frequency of 0.08 Hz, and an average turning rate of 9.08 deg to the right. A more detailed description of the gait can be found in Refs. [12,17]. We compared the measurements between the vendor-recommended offset correction and our calibration; see Supplemental Materials on the ASME Digital Collection.

Table 1 Summary of model selection statistics

Model	DOF	CV error	BIC
Full (six rotations + six translations)	18 + 18	12	1580
Six rotations + single translation	18 + 3	17	1674
Six translations only	18	62	2352
Single translation	3	105	2546

Abbreviations: degree-of–freedom (DOF), cross-validation (CV), and Bayesian information criterion (BIC).

6 Discussions

In this paper, we showed that naive offset correction of the measurements from the six 6-axis transducers on our hexapedal robot in a static pose produced horizontal force estimates of the order of 25% of mg, and pitch and roll torque ranges that do not even contain the true torque of 0 (see Fig. 2). The poor accuracy of this ground contact wrench measurement hindered us from studying our model of multilegged walking and slipping.

To resolve this we showed an in situ calibration framework for these sensors which can be used without disassembling the robot. We characterized transducer offset, leg gravity offset and the wrench transformation error in our model.

We first estimated transducer offset and leg gravity offset by hanging the robot in two sets of opposite directions. Our calibration method took into account of a hanging orientation error $\hat{\mathbf{s}}$ when solving for the transducer offset and tool gravitational offset. Without this $\hat{\mathbf{s}}$ the residual error had a multimodal distribution (see Fig. 5), especially in Fx and Fy. By characterizing an infinitesimal rotation error $\hat{\mathbf{s}}$ during the hanging experiment, the error distributions became more similar to a zero mean normal distribution, with a maximum 0.2 N standard deviation.

In our second calibration step, we characterized the frame transformation estimation error between the transducer frame and the body frame together with the unknown translation between the body frame origin and the CoM. The unknown translation between the body frame origin and the CoM removed the 2.5 Nm bias in torque estimation. Using the frame transformation correction, we reduced the 5-fold cross-validation residual by a factor of $\times 8$ compared with only fitting a single translation transformed to the CoM. Overall, the calibration framework enabled us to make a much more accurate measurement of ground contact forces and the ensuing leg wrenches.

We also noticed that the offset term on the transducer could change. Our experience showed the offset changed up to 10 N after 6 months. Temperature change and gauge excitation voltage could be possible causes for the drift, and thus should be expected over extended periods [26]. When such a significant offset change occurred, we easily re-estimated $\mathbf{w}_o^{\text{ft}_k}$ by putting it as the optimization variables in Eq. (8), with the other calibration parameters held unchanged. This only required a few measurements with the robot standing at different poses. We found no need to redo the entire protocol of hanging experiments to adjust this calibration.

This calibration procedure can be generalized to other systems that have a tool attached to an F/T transducer. For example, when an F/T transducer is attached between the end of a manipulator and an actuated tool head, one can estimate the transducer offset and tool gravity offset by following the same procedure described in Sec. 4.1. However, instead of hanging, one should set the manipulator joint angles to position the tool in opposite orientations. The $\hat{\mathbf{s}}$ term can compensate for imperfect opposite orientations, and the method used to characterize the leg CoM can be applied to determine the tool CoM during actuation.

The Cayley transformation parametrization used in Sec. 4.2 is a powerful technique to switch the optimization argument set from a rotation group to a vector space. It can be used to characterize unknown rotation matrices in general, as long as one can formulate an objective function to optimize toward.

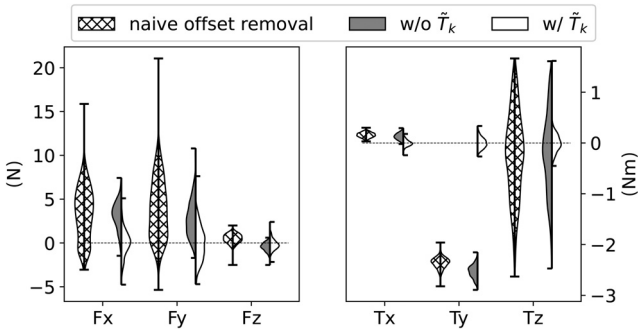

Fig. 6 Violin plot of the residual of the sum of force (left) and torque (right) at robot CoM in floating base frame at different poses. Naive bias removal (cross hatch filling), without characterizing transformation error (gray filling), our calibration method with $(\mathbf{R}_k, \mathbf{p}_k)$ (white filling). Our calibration reduced the RSME (from cross hatch to white) by 63% for forces (66% in Fx, 61% in Fy, 13% in Fz) and 90% for torques (61% in Tx, 95% in Ty, 78% in Tz).

7 Conclusion

We have demonstrated a calibration methodology that enabled us to simultaneously measure the ground contact wrenches in a six-legged robot while it is walking and its legs are slipping. We used the data thus obtained in Ref. [27], which discusses the multilegged locomotion model with its predictions, and suggests some explanations as to why a non-Coulomb friction model is successful at predicting motion governed by Coulomb friction.

Acknowledgment

This work was supported by D. Dan and Betty Kahn Michigan-Israel Partnership for Research and Education Autonomous Systems Mega-Project.

Funding Data

- ARO (Award IDs. MURI W911NF-17-1-0306, W911NF-17-1-0243, and W911NF-14-1-0573; Funder ID: 10.13039/100000183).
- NSF (Award ID. CPS 2038432; Funder ID: 10.13039/100000144).

Data Availability Statement

The datasets generated and supporting the findings of this article are obtainable from the corresponding author upon reasonable request.

References

[1] Cao, M. Y., Laws, S., and Baena, F. R. y., 2021, "Six-Axis Force/Torque Sensors for Robotics Applications: A Review," IEEE Sens. J., **21**(24), pp. 27238–27251.
[2] Schwalb, W., Shirinzadeh, B., and Smith, J., 2017, "A Force-Sensing Surgical Tool With a Proximally Located Force/Torque Sensor," Int. J. Med. Rob. Comput. Assisted Surg., **13**(1), p. e1737.
[3] Shimano, B., and Roth, B., 1977, "On Force Sensing Information and Its Use in Controlling Manipulators," IFAC Proc. Vol., **10**(11), pp. 119–126.
[4] Howe, R. D., 1993, "Tactile Sensing and Control of Robotic Manipulation," Adv. Rob., **8**(3), pp. 245–261.
[5] Hutter, M., Gehring, C., Lauber, A., Gunther, F., Bellicoso, C. D., Tsounis, V., Fankhauser, P., et al., 2017, "Anymal - Toward Legged Robots for Harsh Environments," Adv. Rob., **31**(17), pp. 918–931.
[6] Komsuolu, H., Sohn, K., Full, R. J., and Koditschek, D. E., 2009, "A Physical Model for Dynamical Arthropod Running on Level Ground," *Experimental Robotics*, O. Khatib, V. Kumar, and G. J. Pappas, eds., Springer, Berlin, Heidelberg, pp. 303–317.
[7] Wu, X. A., Huh, T. M., Mukherjee, R., and Cutkosky, M., 2016, "Integrated Ground Reaction Force Sensing and Terrain Classification for Small Legged Robots," IEEE Rob. Autom. Lett., **1**(2), pp. 1125–1132.
[8] Lin, P.-C., Komsuoglu, H., and Koditschek, D., 2005, "A Leg Configuration Measurement System for Full-Body Pose Estimates in a Hexapod Robot," IEEE Trans. Rob., **21**(3), pp. 411–422.
[9] Kim, J.-H., 2020, "Multi-Axis Force-Torque Sensors for Measuring Zero-Moment Point in Humanoid Robots: A Review," IEEE Sens. J., **20**(3), pp. 1126–1141.
[10] Saranli, U., Buehler, M., and Koditschek, D. E., 2001, "Rhex: A Simple and Highly Mobile Hexapod Robot," Int. J. Rob. Res., **20**(7), pp. 616–631.
[11] Fitzner, I., Sun, Y., Sachdeva, V., and Revzen, S., 2017, "Rapidly Prototyping Robots: Using Plates and Reinforced Flexures," IEEE Rob. Autom. Mag., **24**(1), pp. 41–47.
[12] Zhao, D., and Revzen, S., 2020, "Multi-Legged Steering and Slipping With Low DoF Hexapod Robots," Bioinspiration Biomimetics, **15**(4), p. 045001.
[13] Zhao, D., Bittner, B., Clifton, G., Gravish, N., and Revzen, S., 2022, "Walking is Like Slithering: A Unifying, Data-Driven View of Locomotion," Proc. Natl. Acad. Sci., **119**(37), p. e2113222119.
[14] Bittner, B. A., Hatton, R. A., and Revzen, S., 2018, "Geometrically Optimal Gaits: A Data-Driven Approach," Nonlinear Dyn., **94**(3), pp. 1933–1948.
[15] Ostrowski, J., and Burdick, J., 1998, "The Geometric Mechanics of Undulatory Robotic Locomotion," Int. J. Rob. Res., **17**(7), pp. 683–701.

[16] Shapere, A., and Wilczek, F., 1987, "Self-Propulsion at Low Reynolds Number," Phys. Rev. Lett., **58**(20), pp. 2051–2054.
[17] Zhao, D., 2021, "Locomotion of Low-Dof Multi-Legged Robots," Ph.D. thesis, University of Michigan, Ann Arbor, MI.
[18] Kao, C.-J., Chen, C.-S., and Lin, P.-C., 2019, "Reactive Force Analysis and Modulation of the Individual Legs in a Running Hexapod Robot," 2019 IEEE/ASME International Conference on Advanced Intelligent Mechatronics (AIM), Hong Kong, China, July 8–12, pp. 370–375.
[19] Chavez, F. J. A., Traversaro, S., Pucci, D., and Nori, F., 2016, "Model Based in Situ Calibration of Six Axis Force Torque Sensors," 2016 IEEE-RAS 16th International Conference on Humanoid Robots (Humanoids), Cancun, Mexico, Nov. 15–17, pp. 422–427.
[20] ATI Industrial Automation, 2021, F/T Transducer Six–Axis Force/Torque Sensor System Installation and Operation Manual, ATI, Apex, NC, accessed June 4, 2024, https://www.ati-ia.com/app_content/documents/9620-05-CTL.pdf
[21] Traversaro, S., Pucci, D., and Nori, F., 2015, "In Situ Calibration of Six-Axis Force-Torque Sensors Using Accelerometer Measurements," 2015 IEEE International Conference on Robotics and Automation (ICRA), Seattle, WA, May 26–30, pp. 2111–2116.
[22] Ding, C., Han, Y., Du, W., Wu, J., and Xiong, Z., 2022, "In Situ Calibration of Six-Axis Force–Torque Sensors for Industrial Robots With Tilting Base," IEEE Trans. Rob., **38**(4), pp. 2308–2321.
[23] Yu, Y., Shi, R., and Lou, Y., 2022, "Bias Estimation and Gravity Compensation for Wrist-Mounted Force/Torque Sensor," IEEE Sens. J., **22**(18), pp. 17625–17634.
[24] Thrun, S., Burgard, W., and Fox, D., 2005, *Probabilistic Robotics (Intelligent Robotics and Autonomous Agents)*, The MIT Press, Cambridge, MA.
[25] Courant, R., and Hilbert, D., 1937, *Methods of Mathematical Physics*, Vol 1, Interscience Publishers, INC, New York.
[26] ATI Industrial Automation, 2019, "Frequently Asked Questions About Force/Torque Sensors," ATI, Apex, NC, accessed June 4, 2024, https://www.ati-ia.com/library/documents/FT_FAQ.pdf
[27] Wu, Z., Zhao, D., and Revzen, S., 2024, "Modeling Multi-Legged Robot Locomotion With Slipping and Its Experimental Validation," Int. J. Rob. Res., (accepted).